

EFFECT OF SILICA SURFACE ON LUMINESCENCE PROPERTIES OF Tb³⁺-GLUTAMIC ACID

J. Jorge¹, M. Vereslt², GR. Castro³ and MAU. Martines^{1*}

¹QI-CCET - Universidade Federal de Mato Grosso do Sul, Av. Felinto Müller, 1555, CEP 79074-460, Campo Grande, MS, Brazil.

²Centre d'Elaboration de Matériaux et d'Etudes Structurales, Université de Toulouse, 29 rue Jeanne Marvig, BP 94347, 31055 Toulouse, Cedex 4, France.

³IBB, Universidade Estadual Paulista, P.O.Box 510, CEP 18618-000, Botucatu, SP, Brazil.

ABSTRACT

We studied the effect of silica surface on luminescence properties of terbium complex by spectroscopy characterization, where microparticles of mesoporous silica type MSU-X was prepared. We used silica with different surface: calcined, washed, functionalized with 3-aminopropyl-triethoxysilane (APTES), and 3-glycidoxypropyl-trimethoxysilane (GPTMS); impregnated with Tb³⁺-glutamic acid complex. The obtained materials were characterized by scanning electron microscopy, porosity measurements, small-angle X-ray scattering, as structural characterization; Fourier transform infrared and luminescence spectroscopy, as spectroscopy characterization. Finally, we observed that functional groups at the silica surface lead to changes on luminescent properties of the final materials. The observed shift of the absorption and emission bands can be assigned to the effect of the functional groups of mesoporous silica.

Keywords: Lanthanide ions, 3-amino-propyl-triethoxysilane, 3-glycidoxy-propyl-trimethoxysilane.

INTRODUCTION

Mesopores, this technical term is applied to porous with diameter size between micro and macro scale, range from 2 to 50 nm^{1, 2}. Mesoporous silica is an excellent matrix host for biomolecules because it has the following features: ordered pores; narrow distribution size pore; high specific surface area, range from 500 to 1300 m².g⁻¹; high pore volume, range from 45 to 75 %; high mechanical and thermal resistance and low hydrothermal resistance. These features make these materials very promising for several applications in industry scale, chemical engineering, environmental, medicine and biology; for example, catalysis³; adsorption of heavy metals (environmental decontamination) and ultrafiltration membranes^{4, 5}; gas storage³; HPLC columns⁶; and for the purposes of our research group, drug delivery⁷; materials for bone regeneration and tissue⁸; self-diagnostic kits; and where is attached the objective of this work, developing of biomarkers³.

In order to build a biomarker using mesoporous silica, a luminescent complex attached inside its porous is needed, in that way as interesting alternative for the biomarkers in use today; the lanthanide ions complex could be hosted. They are interesting luminescent centers due to their photostability and to several peculiar emission characteristics, such as narrow lines; large Stokes' shifts; long decay times. Lanthanide complexes, grafted on, or supported by silica nanoparticles have been proposed for the development of immunoassay techniques, DNA detection and specific marker mainly due the easy modification of micro and nano particles surfaces of mesoporous silica⁹.

Tb³⁺ is luminescent in aqueous solution, and generally retains their luminescence when bound to complex ligand systems. Furthermore, exhibit multiple emissions (due to several electronic transitions) whose relative intensities and line splitting patterns (band structuring) are sensitive to the detailed nature of the ligand environment about the metal ion. The luminescence properties of Tb³⁺ make this ion

obvious candidate for use as luminescent probes of metal binding in biomolecular systems¹⁰.

Therefore we came to our work's purpose which is spectroscopic properties of Tb³⁺ - L-glutamic acid complex impregnated into channels of mesoporous silica were studied as an effect of chemical modification of silica surface. Looking forward the use of luminescent materials as promising alternative for the biomarkers in use today.

EXPERIMENTAL SECTION

All reagents were purchased from Aldrich and Fluka and used as received. The experimental section consisted in the acquisition of microparticles by mixing Tween 60 surfactant, water and chloride acid (HCl) to set to 2 the pH, after this tetraethyl orthosilicate (TEOS) was added as the silica precursor and the mix was kept still at room temperature hydrolysis without stirring for 12 h, then the reaction's catalyst sodium fluoride (NaF) was added and the reaction remained in condensation for 72 h and 65°C under stirring, elapsed this time the obtained precipitate was filtered⁴. In this research it has been used silica with different surfaces: calcined silica at 600°C for complete removal of the surfactant, named calcined silica; washed silica in Soxhlet extractor to the same purpose, named washed silica; functionalized silica with APTES (3-aminopropyltriethoxysilane), named APTES functionalized silica; functionalized silica with GPTMS (3-glycidoxypropyltrimethoxysilane), named GPTMS functionalized silica, in order to couple functional groups.

5.0 g of mesoporous silica were dried at 150°C under vacuum for 24 h, after mixed with 70 ml DMF¹¹. The pre-hydrolysis reaction of APTES was performed with 19.3 ml distilled water, 1.9 ml HCl (0.01 mol.L⁻¹) and 22.5 ml APTES, by 1 h under magnetic stirring. After this, the solution was added to silica with DMF for functionalization. The reaction remained in reflux for 72 h at 120°C.

The same proceeding was adopted for silica functionalization with GPTMS. The amount used here were: 3.0 g of mesoporous silica, 41.3 ml DMF, 83 ml distilled water, 8.32 ml HCl (0.01 mol.L⁻¹) and 10.98 ml GPTMS.

All these silica were impregnated with the Tb³⁺ - L-glutamic acid complex as a ligand. The Terbium's solution was prepared using solvent ethanol; the solution's concentration was 5 x 10⁻² mol.L⁻¹. The L-glutamic acid solution was prepared using solvent ethanol; the concentration of solution was 2 x 10⁻¹ mol.L⁻¹. After this step, the L-glutamic acid solution was added to Tb³⁺ solution (1:1), like as¹², for complete formation of lanthanide-amino acid complex.

The impregnation of luminescent complex in silica was performed by addition of 5.0 ml pure luminescent complex to 0.15 g mesoporous silica, the mix was kept under stirring for solubilization for 8 h, after this was washed 3 times and dried at 50°C, for removal of excess of the luminescent complex.

The obtained material passed through the following characterization techniques: Scanning Electron Microscopy (SEM) to observe morphology and size of the particles, in electronic microscope JEOL SJM 6490. Porosity measurements to collect information about surface area and pores diameter, Nitrogen absorption isotherms were measured at 77 K with a Micromeritics 2010 instrument using standard procedures. Surface areas were determined by the Brunauer-Emmett-Teller (BET) method within a relative pressure range of 0.05–0.2. Pore size distributions were calculated only for sizes above 2.5 nm from the desorption branch, using a polynomial correlation between relative pressure and pore diameter deduced from the Broekhoff and Boer (BdB) model^{13, 14}. To facilitate comparisons, the reduced adsorption curves (isotherms divided by the amount adsorbed at a relative pressure of 0.8) were displayed¹⁵. The absorption effect was corrected for all the samples. Small-angle X-ray scattering (SAXS) in order to analyze pores arrangement and organization, measured on National Laboratory Synchrotron Light (LNLS Campinas, Brazil), was used asymmetric slit and silicon monochromator (111), with monochromatic beam ($\lambda = 1.488 \text{ \AA}$) and horizontal focus. The scattered intensity was collected with "imaging plate" at 849.64 mm of the sample.

The camera length corresponds to a scattering vector q ranging from 0.018 to 0.39 \AA^{-1} . Horizontal and vertical beam stoppers were used to absorb the direct and the totally reflected X-ray beam, respectively. Most of the patterns exhibited single diffraction peaks that were assigned to a pore correlation length. This pore center to pore center correlation length is herein after referred to as "d-spacing". Fourier Transform Infrared (FT-IR) spectra were acquired within the 4000 to 500 cm^{-1} range using KBr pellets with a 2 cm^{-1} resolution, using a BOMEM MB 100 spectrometer, for to observe the efficacy of wash and calcination of silica as well the functionalization of this. Luminescence spectroscopy, to study luminescence properties and possible interactions between complex and surface, was recorded with a spectrofluorimeter Horiba Jobin-Yvon FluoroLog-3 with xenon lamp of 450 W as excitation source, monochromator iHR-320, under the same instrumental conditions for all samples. The signals were normalized by excitation lamp power, and the emissions were corrected. For

luminescence decay, a pulsed 3 μs with xenon lamp was used. Except for excitation wavelengths, the data acquisition parameters were the same for all samples: integration time between pulses of 2 ms, initial delay of 0.05 ms, maximum delay of 2.00 ms, cycling time of 41 ms, number of pulses of 200 per cycle. The samples of silica were used in solid state and the luminescent complex of Tb^{3+} with L-glutamic acid was used in solution.

RESULTS AND DISCUSSION

Start analyzing the experimental results beginning with the SEM; the SEM images (Figure 1) shows particles micrometric size with heterogenic shape, going from sticks to spherical, characteristic of MSU-X type of mesoporous silica. The material was named Michigan State University type material, or MSU-X silica (X refers to the nature of the surfactant: 1 for alkyl-PEO, 2 for alkylaryl-PEO, 3 for polypropyleneoxyde-PEO block copolymer, and 4 for Tween-type nonionic ethoxylated sorbitan esters) is prepared under neutral or mild acidic conditions. The average size was estimated by *ImageJ*¹⁶ and with those measurements was composed a histogram showing the size distribution of the particles, the average size was estimated in 3.3 μm and standard-deviation of 0.91 μm (Figure 2). The final structure and the morphology of MSU-X type material are highly dependent on the parameter of the reaction mean, such as a local interaction created by the lipophilic/hydrophilic equilibrium, the Brownian motion that destroys the network, the hydrolysis kinetic and polymerization of silica. Synthesis of MSU-X type mesoporous silica based on hydrogen bonding illustrates perfectly the versatility of this approach, since the final material structure (pore diameter, particle size) can be readily modified by adjusting several synthesis parameters, with the same reaction medium⁴.

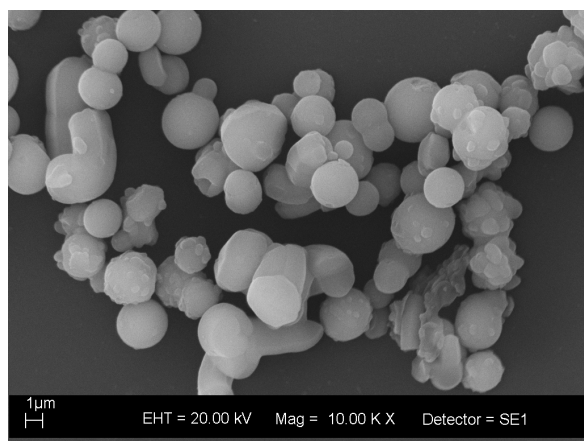


Fig. 1: SEM image of washed pure silica

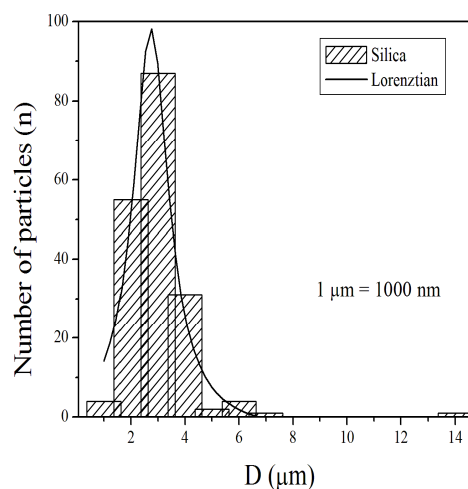


Fig. 2: Diameter rate histogram of particle by number of particle

The porosity measurements' graphic, Figure 3 and 4, shows the Nitrogen adsorption-desorption isotherm at 77K, the hysteresis and shape of the curves reveals mesoporous material characteristics. The graphics inserted shows that surface area was practically unchanged for all the samples, a high specific surface of $1200 \text{ m}^2 \cdot \text{g}^{-1}$, changing just the pores average size: washed silica 35 \AA (Figure 3a); calcined silica 44 \AA (Figure 3b); APTES functionalized 40 \AA (Figure 4a), and GPTMS functionalized 39 \AA (Figure 4b). Therefore, the samples exhibit substantial structure of confined mesoporous. The adsorption isotherm for washed silica no exhibits hysteresis, feature of uniform pores, the adsorption not increase in high relative pressure, feature of textural porosity, like as the curve of adsorption that not exhibits hysteresis, which is characteristic of pore necking. In addition, a parallel trend it's observed for adsorption-desorption isotherm of the other silica, where the curve of adsorption take a significant shift toward high relative pressure, characteristics of larger pores size. The samples shows fine distribution pores, typical of materials template structured (MTS), with type IV nitrogen adsorption-desorption isotherm⁴.

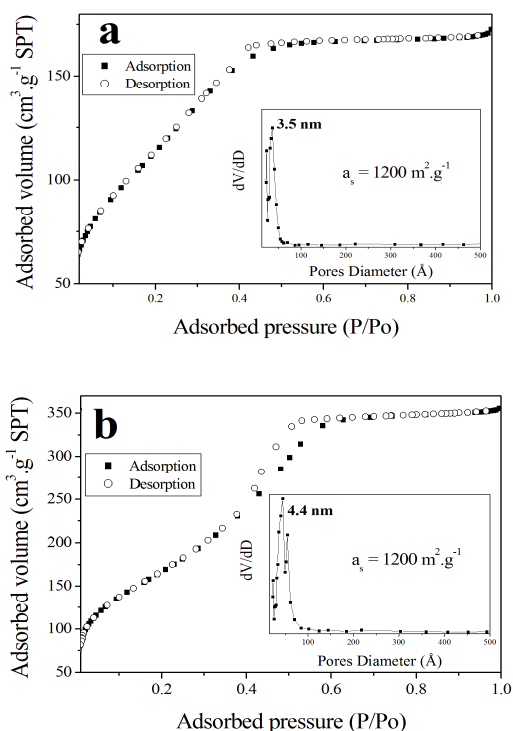


Fig. 3: Adsorption/desorption N2 liquid isotherm of washed (3a), and calcined (3b) mesoporous silica, with distribution pores diameter inserted

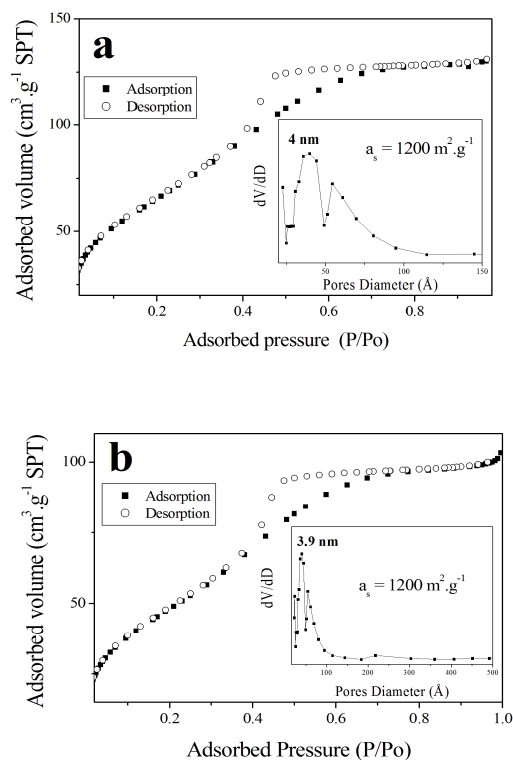


Fig. 4: Adsorption/desorption N2 liquid isotherm of functionalized APTES (4a), and GPTMS (4b) mesoporous silica, with distribution pores diameter inserted

The SAXS measures, Figure 5, were performed in order to collect information about structure and arrangement of pores. A view of the spectra displays the diffraction peak d_1 1 0 0 for washed (a), calcined (b), and GPTMS (d) functionalized silica. The presence of just one diffraction peak, for all the silica, except APTES functionalized silica (c), denotes wormhole porous arrangement material in 3D, ordered mesostructure, and the quality of the sample may be estimated by diffraction line intensity^{14,17}. The wall thickness was estimated by calculation as⁴, using the following: Wall thickness = d spacing – d pore, the values was estimated of 23.0 Å for GPTMS functionalized silica, 35.1 Å for calcined silica, and 16.5 Å for washed silica.

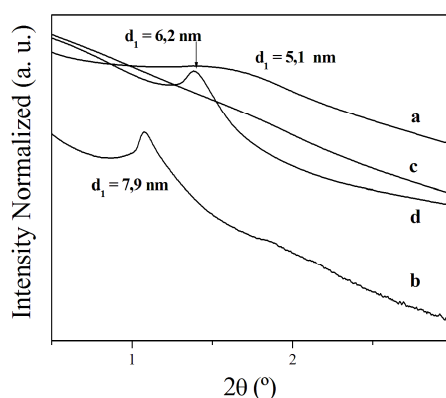


Fig. 5: SAXS of washed silica (a), calcined silica (b), APTES functionalized silica (c), and GPTMS functionalized silica (d)

The IR spectra in Figure 6 are typical of noncrystalline silica, including amine and glycidoxy groups bands. The bands assignments from the spectra are described. Asymmetric stretching Si-O and Si-O-(Si) vibrations occur in the 1233-1041 cm^{-1} wavenumber range. Si-O- asymmetric and SiO symmetric stretchings appear in 957 and 803 cm^{-1} , respectively. Deformation O-Si-O appears at 464 cm^{-1} . All the spectra show typical water molecule stretching bands in the 3622-3323 cm^{-1} region. The water molecule deformation band generally observed about 1625 cm^{-1} appears between 1639 and 1661 cm^{-1} for each sample. This shift to a larger wavenumber can be attributed to the presence of H_3O^+ ions in the silica samples¹⁸. The amine and glycidoxy groups can be detected by IR measurements, in the spectrum of Figure 6c, where two new absorption bands, assigned ascribed to the N-H stretching modes of the primary amine, appear at 3100 cm^{-1} . The bands at 1558 cm^{-1} , attributed to the H-N-H bending (scissoring) vibrations, confirm the

functionalization of the mesoporous silica. In the Figure 6c and 6d, the absorption bands at 2930 and 2850 cm^{-1} , ascribed to symmetric (us) and anti-symmetric (uas) CH_2 stretching, and at 1348, 1390, 1480, 1537 and 1596 cm^{-1} (ascribed to C-H bending) give evidence of aminopropyl and glycidoxypropyl groups functionalized in the mesoporous silica surface^{19, 20}.

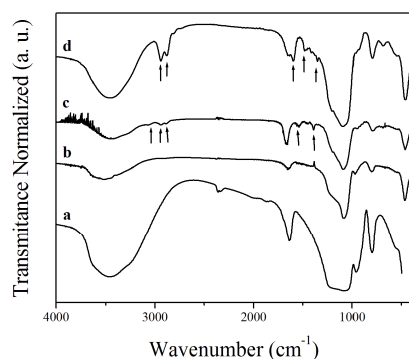


Fig. 6: Fourier Transform Infrared spectra of samples of washed (a), calcined (b), and functionalized GPTMS (c) and APTES (d) silica

The excitation spectra (Figure 7) depict that, for solution's spectrum (a), the peaks which appear between 300 and 500 nm are attributed the $7F_6 \rightarrow 5X_n$ transitions ($7F_6 \rightarrow 5D_4$; $7F_6 \rightarrow 5L_9$; $7F_6 \rightarrow 5L_7$, and $7F_6 \rightarrow 5H_7$, distinguished)²¹⁻²⁵, characteristics of trivalent terbium ion. For the spectra of silica impregnated with the luminescent complex, are noted peaks that not appear for spectrum of the solution indicating ligand-to-metal charge-transfer transition caused by interaction between the luminescent complex and the amine and the glycidoxy groups²⁶.

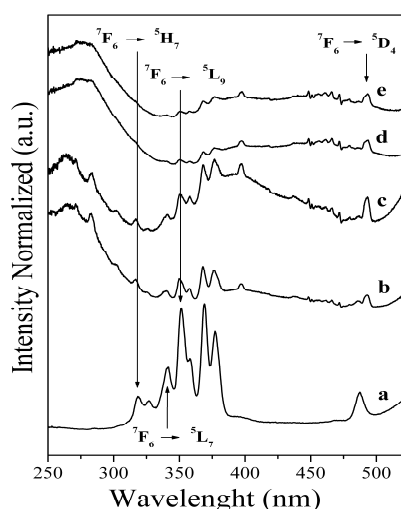


Fig. 7: Spectra of excitation, $\lambda_{\text{em}} = 543\text{nm}$, of Tb^{3+} - L-glutamic acid complex (a);

washed silica (b); calcined silica (c); APTES functionalized silica (d), and GPTMS functionalized silica (e), impregnated with luminescent complex

Emission spectra (Figure 8) shows the characteristics peaks of the transitions energy levels of trivalent Terbium ion $5D_4 \rightarrow 7F_J$ ($J=6, 5$ and 4) over 470 nm²⁵⁻²⁹. The broad peak before the transition first peak might be caused by luminescent complex and silica surface interaction. Furthermore, the low baseline indicates that the Si-O network absorption could be neglected, leaching of the photoactive molecules has been avoided and the effective energy transfer took place between the modified organic ligands and the chelated terbium ion. The mesoporous luminescent materials show relatively strong emission owing to the chemically covalently bonded molecular Si-O network structure between the complex and the mesoporous silica²⁵.

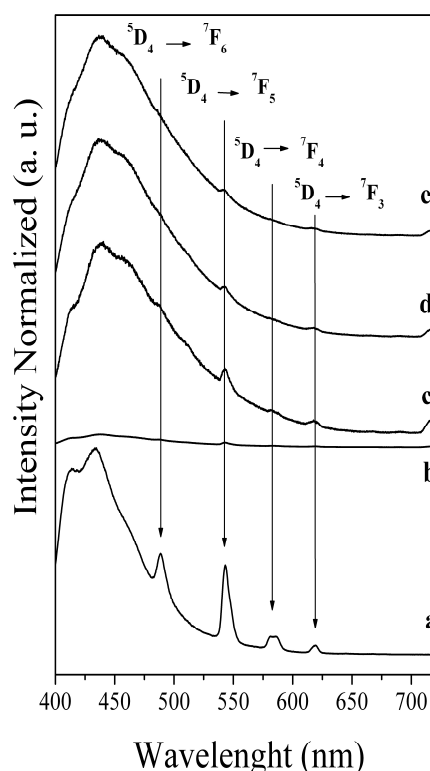


Fig. 8: Spectra of emission, $\lambda_{\text{exc}} = 377\text{nm}$ of Tb^{3+} - L-glutamic acid complex (a); washed silica (b); calcined silica (c); APTES functionalized silica (d), and GPTMS functionalized silica (e), impregnated with luminescent complex.

Studying the lifetime of luminescence curves, Figure 9, it is possible to see unmodified silica, calcined silica (a) and washed silica (b), has

just one lifetime. The only lifetime showed for unmodified silica suggests that Tb ion is occupying just one place.

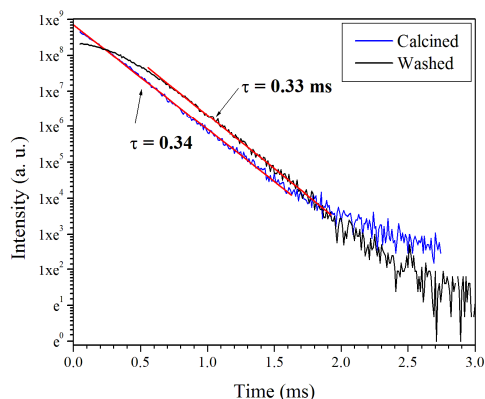


Fig. 9: Decay emission curves for Tb³⁺ ion luminescence (5D₄ → 7F₅ transition) in calcined (a) and washed silica (b) matrix. Spectra were acquired by emission at 543 nm and excitation at 377 nm

Modified silica, APTES functionalized (a) and GPTMS functionalized silica (b), (Figure 10) has two lifetimes. The two lifetimes in modified silica suggests the lanthanide ion occupies two different places, one of them due the adsorption in silica by the complex, and the other due the interaction between silica surface and the complex.

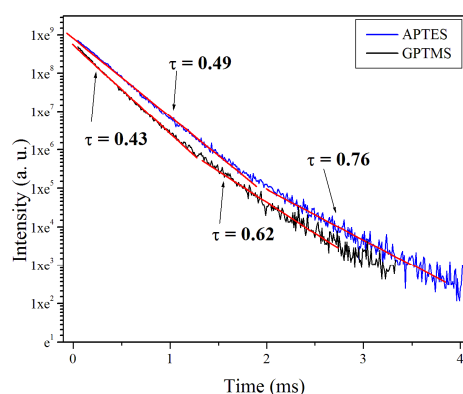


Fig. 10: Decay emission curves for Tb³⁺ ion luminescence (5D₄ → 7F₅ transition) in APTES (a) and GPTMS functionalized silica (b) matrix. Spectra were acquired by emission at 543 nm and excitation at 377 nm

CONCLUSION

Luminescent complexes were attached to microparticles of mesoporous silica, confirmed by excitation and emission spectra which enhances its importance as promising alternative biomarkers. When modifying microparticles surface; shifts on bands of

excitation and emission are noted, also an increase of the lifetime and the appearance of another lifetime.

ACKNOWLEDGEMENT

We would like to thank all governments' agencies and institutions which made possible this research. JJ thanks the CNPq foundation for its fellowship. The authors gratefully acknowledge CNPq, FUNDECT-MS and CAPES-COFECUB for its financial support, and CEMES for the luminescence measurements, the Brazilian Synchrotron Light Laboratory—LNLS for the SAXS, and the National Laboratory of Nanotechnology - LNNano for the SEM measurements.

REFERENCES

1. Sing KSW, Everett DH, Haul RAW, Moscou L, Pierotti RA, Rouquerol J and Siemieniowska T. Reporting Physisorption Data for Gas/Solid Systems with Special Reference to the Determination of Surface Area and Porosity. *Pure Appl Chem.* 1985; 57: 603-619.
2. Rouquerol J, Avnir D, Fairbridge CW, Everett DH, Haynes JM, Pernicone N, Ramsay JDF, Sing KSW and Unger KK. Recommendations for the Characterization of Porous Solids. *Pure Appl Chem.* 1994; 66: 1739-1758.
3. Hoffmann F, Cornelius M, Morell J and Fröba M. Silica-Based Mesoporous Organic-Inorganic Hybrid Materials. *Angew Chem Int Ed.* 2006; 45: 3216-3251.
4. Boissiere C, Martines MAU, Kooyamn PJ, Kruijff TR, Larbot A and Prouzet E. Ultrafiltration Membrane Made with Mesoporous MSU-X Silica. *Chem Mater.* 2003; 15: 460-463.
5. Evangelista SM, DeOliveira E, Castro GR, Zara L.F and Prado AGS. Hexagonal mesoporous silica modified with 2-mercaptothiazoline for removing mercury from water solution. *Surf Sci.* 2007; 601: 2194-2202.
6. Martines MAU, Yeong E, Persin M, Larbot A, Voorhout WF, Kübel CKU, Kooyman P and Prouzet E. Hexagonal mesoporous silica nanoparticles with large pores and a hierarchical porosity tested for HPLC. *CR Chimie.* 2005; 8: 627-634.
7. Cheng SH, Lee CH, Yang CS, Tseng FG, Mou CY and Lo LW. Mesoporous silica nanoparticles functionalized with an oxygen-sensing probe for cell photodynamic therapy: potential cancer

- theranostics. *J Mater Chem.* 2009; 19: 1252-1257.
8. Shi Q, Wang J, Zhang J, Fan J and Stucky GD. Rapid-Setting, Mesoporous, Bioactive Glass Cements that Induce Accelerated In Vitro Apatite Formation. *Adv Mater.* 2006; 18: 1038-1042.
 9. Yan J, Estevez CM, Smith JE, Wang KM, He XX, Wang L and Tan WH. Dye-doped nanoparticles for bioanalysis. *Nano Today.* 2007; 2: 44-50.
 10. Richardson FS. Terbium(III) and Europium(III) Ions as Luminescent Probes and Stains for Biomolecular Systems. *Chem Rev.* 1982; 82: 541-552.
 11. Pereira AS, Ferreira G, Caetano L, Martines MAU, Padilha P.M, Santos A and Castro GR. Preconcentration and determination of Cu(II) in a fresh water sample using modified silica gel as a solid-phase extraction adsorbent. *J Hazard Mater.* 2010; 175: 399-403.
 12. Jericó S, Carubelli CR, Massabni AMG, Stucchi EB, Leite SRA and Malta O. Spectroscopic Study of Interaction of Nd³⁺ with Amino Acids: Phenomenological 4f-4f Intensity Parameters. *J Braz Chem Soc.* 1998; 9: 487-493.
 13. Broekhoff JCP and de Boer JH. Studies on Pore Systems in Catalysts. XVIII – Pore Distributions from the Desorption Branch of a Nitrogen Sorption Isotherm in the Case of Cylindrical Pores. B – Applications. *J Catal.* 1968; 10: 377-390.
 14. Prouzet E, Cot F, Nabias G, Larbot A, Kooyman P and Pinnavaia TJ. Assembly of Mesoporous Silica Molecular Sieves Based on Nonionic Ethoxylated Sorbitan Esters as Structure Directors. *Chem Mater.* 1999; 11: 1498-1503.
 15. Ryoo R, Ko CH, Kruk M, Antochshuk V and Jaroniec M. Block-Copolymer-Templated Ordered Mesoporous Silica: Array of Uniform Mesopores or Mesopore-Micropore Network? *J Phys Chem B.* 2000; 104: 11465-11471.
 16. Abramoff MD, Magalhaes PJ and Ram SJ. Image processing with ImageJ. *Biophotonics International.* 2004; 11: 36-42.
 17. Prouzet E and Pinnavaia TJ. Assembly of Mesoporous Molecular Sieves Containing Wormhole Motifs by a Nonionic Surfactant Pathway: Control of Pore Size by Synthesis Temperature. *Angew Chem Int Ed.* 1997; 36: 516-518.
 18. Martines MAU, Pecoraro E, Simoneti JA, Davolos MR and Jafelicci JrM. Effects of Different Treatments on Purity of Silica from Soluble Sodium Silicate. *Separ Sci Technol.* 2000; 35: 287-298.
 19. Silverstein RM, Webster FX and Kiemle DJ. *Spectrometric identification of Organic Compounds*; John Wiley & Sons: New York, NY, USA, 2005; p. 502.
 20. Pavia DL, Lampman GM, Kriz GS and Vyvyan JR. *Introduction to Spectroscopy*; Brooks/Cole: Belmont, CA, USA, 2009; p. 656.
 21. Yang J, Li GG, Peng C, Li CX, Zhang CM, Fan Y, Xu ZH, Cheng ZY and Lin J. Homogeneous one-dimensional structured Tb(OH)₃:Eu³⁺ nanorods: Hydrothermal synthesis, energy transfer, and tunable luminescence properties. *J Solid State Chem.* 2010; 183: 451-457.
 22. Martínez-Martínez R, Álvarez E, Speghini A, Falcony C and Caldiño U. White light generation in Al₂O₃:Ce³⁺:Tb³⁺:Mn²⁺ films deposited by ultrasonic spray pyrolysis. *Thin Solid Films.* 2010; 518: 5724-5730.
 23. Pedrini C, Belsky A, Ivanovskikh KV, Petrosyan AG, Sargsyan RV and Kamenskikh I. Cerium-, praseodymium- and terbium-trapped excitons in oxides. *Chem Phys Lett.* 2011; 515: 258-262.
 24. Caird JA, Carnall WT, Hessler JP and Williams CW. The terbium chloride-aluminum chloride vapor system. I. Absorption and excitation spectra. *J Chem Phys.* 1981; 74: 798-804.
 25. Yan ZZ, Tang Y, Liu WS and Tan MY. Preparation and luminescent properties of silica-based composite materials encapsulating a novel terbium complex. *Solid State Sci.* 2008; 10: 332-336.
 26. Li YJ, Yan B and Wang L. Rare earth (Eu³⁺, Tb³⁺) mesoporous hybrids with calix[4]arene derivative covalently linking MCM-41: Physical characterization and photoluminescence property. *J Solid State Chem.* 2011; 184: 2571-2579.
 27. Sivakumar S, Diamente PR and van Veggel FCJM. Silica-Coated Ln³⁺-Doped LaF₃ Nanoparticles as Robust Down- and Upconverting Biolabels. *Chem Eur J.* 2006; 12: 5878-5884.
 28. Wang YG, Li HR, Zhang WJ and Liu BY. Luminescence properties of nanozeolite L grafted with terbium organic complex. *Mater Lett.* 2008; 62: 3167-3170.

29. Josse D, Xie WH, Renault F, Rochu D, Schopfer LM, Masson P and Lockridge O. Identification of Residues Essential for Human Paraoxonase (PON1) Arylesterase/Organophosphatase Activities. *Biochemistry.* 1999; 38: 2816-2825.